J Mol Model (2015) 21: 93
DOI 10.1007/s00894-015-2593-5

ORIGINAL PAPER

Understanding the azeotropic diethyl carbonate–water mixture by structural and energetic characterization of DEC$(H_2O)_n$ heteroclusters

Juan D. Ripoll · Sol M. Mejía · Matthew J. L. Mills · Aída L. Villa

Received: 16 December 2014 / Accepted: 26 January 2015 / Published online: 19 March 2015

Abstract Diethyl carbonate (DEC) is an oxygenated fuel additive. During its synthesis through a promising green process, a DEC-water azeotrope is formed, which decreases DEC production efficiency in the gas phase. Molecular information about this system is scarce but could be of benefit in understanding (and potentially improving) the synthetic process. Therefore, we report a detailed computational study of the conformers of DEC, and their microsolvation with up to four water molecules, with the goal of understanding the observed 1:3 DEC:H_2O molar ratio. The most stable DEC conformers (with mutual energy differences < 1.5 kcal mol^{-1}) contribute to the energetic and structural properties of the complexes. An exhaustive stochastic exploration of each potential energy surface of DEC-$(H_2O)_n$, (where n=1, 2, 3, 4) heteroclusters discovered 3, 8, 7, and 4 heterodimers, heterotrimers, heterotetramers, and heteropentamers, respectively, at the MP2/6-311++G(d,p) level of theory. DEC conformers and energies of the most stable structures at each heterocluster size were refined using CCSD(T)/6-311++G(d,p). Energy decomposition, electron density topology, and cooperative effects analyses were carried out to determine the relationship between the geometrical features of the heteroclusters and the non-covalent interaction types responsible for their stabilization. Our findings show that electrostatic and exchange energies are responsible for heterocluster stabilization, and also suggest a mutual weakening among hydrogen bonds when more than three water molecules are present. All described results are complementary and suggest a structural and energetic explanation at the molecular level for the experimental molar ratio of 1:3 (DEC:H_2O) for the DEC-water azeotrope.

Keywords Oxygenated fuel-water azeotrope · Non-covalent interaction · Stochastic exploration · Electron density topology · Cooperative effect

Electronic supplementary material The online version of this article (doi:10.1007/s00894-015-2593-5) contains supplementary material, which is available to authorized users.

J. D. Ripoll · A. L. Villa
Environmental Catalysis Research Group, Chemical Engineering Department, Engineering Faculty, Universidad de Antioquia, Calle 70 No. 52-21, Medellin, Colombia

S. M. Mejía (✉)
Grupo de Investigación Fitoquímica Universidad Javeriana (GIFUJ), Departamento de Química, Facultad de Ciencias, Pontificia Universidad Javeriana, Carrera 7 No. 40-62, Bogotá, D. C., Colombia
e-mail: sol.mejia@javeriana.edu.co

M. J. L. Mills
Deconstruction Division, Joint BioEnergy Institute, Emeryville, CA, USA

M. J. L. Mills
Biomass Science and Conversion Technology Department, Sandia National Laboratories, Livermore, CA, USA

Introduction

The environmental and energy problems that arise in the world today increasingly attract the attention of many researchers. For instance, the greenhouse effect is generally related to CO_2 emissions generated by the burning of fossil fuels, which are non-renewable energy resources [1–3]. Therefore, it is pertinent to continue obtaining more and diverse knowledge about alternative renewable fuels, as well as suitable avenues toward both decreasing current levels of fossil fuel consumption, and decreasing the associated emission of volatile organic compounds and pollution [4–6].

Several studies have shown that reduction of undesirable emissions, such as soot, unburned hydrocarbons and CO, produced by combustion engines can be achieved by the use of oxygenated fuel additives [7–9]. Some linear carbonates can be used in such a role due to the high oxygen percentage in

their chemical structures and also to their high miscibility with fossil fuels [10, 11].

This is the case for diethyl carbonate (DEC)—an organic compound that can be synthesized from CO_2 (or CO) and ethanol using environmentally friendly processes and an appropriate catalyst [12–14]. This reaction is reversible in the gas phase (in which the reaction is carried out) and, notably, the DEC yield may be enhanced by removing water from the reaction products. For the DEC production and purification process, it is therefore necessary to note and consider the presence in the reaction mixture of both the DEC-water azeotrope: 70 %m/m in DEC at 91 °C [15], (DEC:H_2O molar ratio: 1:3), and the ethanol-water azeotrope: 96 %m/m in ethanol at 78.3 °C [16, 17], (CH_3CH_2OH:H_2O molar ratio: 9:1).

Significant information related to the ethanol-water azeotrope is available from both experimental and computational studies [18–28]. On the one hand, it has been reported that the most stable ethanol conformers are the trans and gauche structures [27] and, interestingly, that the ethanol-water azeotrope is not affected significantly by changes in pressure [28]. On the other hand, O–H···O hydrogen bonds (HBs) strengthened by cooperative effects are responsible for the geometric preferences of $(ethanol)_n$-water (where n=1, 2, 3, 4, and 5) heteroclusters [19, 29, 30], but those same interactions and their spatial arrangements are also observed for $(methanol)_n$-water (where n=1, 2, 3, 4, and 5) heteroclusters [19, 22]—a system that does not form an azeotrope. Even considering protonated water instead of a water molecule, it has been suggested that the respective most stable structure for both $(ROH)_9H_3O^+$ heteroclusters (i.e., R = CH_3–, CH_2CH_3–) consists of three fused five-membered rings. Each ring is formed by four alcohol molecules and a H_3O^+ cation, where the protonated water acts as double proton donor in two of the five HBs in each five-membered ring [31, 32]. To summarize, there is no difference between the neutral and charged alcohol-water systems at a molecular level when the O–H···O HBs are considered until nine ethanol molecules are present. However, the azeotrope's stability may be attributed to the higher abundance of C–H···O weak interactions when compared to stronger O–H···O HBs.

In contrast to the ethanol and methanol systems, to the best of our knowledge there is a lack of information at the molecular level for the DEC-H_2O azeotrope. Therefore, there is a great opportunity to enhance our knowledge of this system, in particular by study of the minimal chemical system that corresponds to the molar ratio found experimentally for the DEC-H_2O (1:3) azeotrope. Understanding the structural characteristics of DEC-$(H_2O)_n$ heteroclusters, and analyzing the nature of the intermolecular forces responsible for their stability could constitute a basis for proposing potential water extraction strategies using, for example, selective membranes in the reaction system during DEC production. Similar ideas have been taken into account to carry out a computational scientific study of metal organic frameworks that can selectively adsorb water from ethanol-water mixtures since this mixture is an azeotrope at 96%m/m in ethanol [18].

One of the purposes of this research was to implement and validate an interface for the ASCEC stochastic method (simulated annealing with quantum energy [33]) with the GAMESS program [34]. The resulting ASCEC-GAMESS program was employed in the exploration of the potential energy surfaces (PES) of DEC-$(H_2O)_n$ heteroclusters (specifically with n=1, 2 ,3, and 4). Reasonable geometric patterns at each cluster size were recognized and the stable heteroclusters were characterized structurally and energetically via geometric and topological data.

Computational methods

Conformational preferences of the DEC molecule were identified by computing the rotational profiles for R–O–C=O and C–C–O–C dihedral angles at the MP2/6-311++G(d,p) level of theory. This level was chosen because its predictions compare favorably with experimental results obtained for both pure dimethyl carbonate (DMC) and DMC-water heterodimer conformations [35]—the latter being an analog of the DEC-water system. This work is intended for publication in a future manuscript.

A modified ASCEC program was employed to generate candidate structures of DEC-$(H_2O)_n$ (n=1, 2, 3, 4) heteroclusters through stochastic exploration of the PES at the B3LYP/6-31+G(d) level of theory. This DFT level has been recommended as the minimum approach for hydrogen-bonded systems [30, 36]. We chose to work with n=3 because this relationship corresponds to the minimal molecular relation that can represent the experimental molar ratio reported for the azeotrope DEC:H_2O (1:3). In addition, we also worked with n=1, 2 and 4 to compare energetic and structural differences due to the presence of numbers of water molecules corresponding to ratios above and below the experimental molar ratio.

The ASCEC program is an implementation of the simulated annealing algorithm with quantum energy, where the random acceptance parameter was modified and the energy was evaluated with quantum methods. The algorithm has been used successfully to study complicated energy landscapes that feature a wide variety of interactions including hydrogen-bonding networks [37–39] and microsolvation of different species [40–43].

An interface with the GAMESS program [34] was written for and is utilized in this report. The code is available by contacting the authors of this report in addition to the authors of the ASCEC program [33].

The B3LYP/6-31+G(d) level of theory was used to calculate the energy of randomly generated cluster configurations.

A geometrical quenching route with an initial temperature of 500K was used, and a constant temperature decrease of 5 % for a total of 100 temperatures. The n water molecules and single DEC molecule were placed at the same position inside cubes. The cube length was settled as 5, 6, 7, and 8 Å for n=1, 2, 3, and 4, respectively. The intramolecular geometry was not allowed to vary during the structure generation. The annealing was run three times for each heterocluster size PES with the same set of parameters and, in some cases, the stochastic sampling generated up to 300 candidate structures on the same PES. This choice of methodology is a good compromise between computational cost and accuracy for the calculation of molecular properties of sizable organic molecules.

Employing the Gaussian09 [44] program, the 932 (DEC(H_2O): 74, DEC(H_2O)$_2$: 332, DEC(H_2O)$_3$: 277, DEC(H_2O)$_4$: 249) candidate structures generated with ASCEC were subjected to a geometry optimization process at the B3LYP/6-31+G(d) level of theory. Subsequently, in order to assess the effect of electron correlation in our calculations, the resulting 34 stable geometries at B3LYP/6-31+G(d) were re-optimized and characterized as minima through analytical frequency calculations at the MP2/6-311++G(d,p) level of theory, resulting in 22 minimum energy structures. The energetic values (relative energies and interaction energies) were corrected with the counterpoise method [45] to estimate the basis set superposition error (BSSE) besides the vibrational zero point energy [46]. In addition, a single point energy calculation with the highly correlated CCSD(T)/6-311++G(d,p)//MP2/6-311++G(d,p) method was carried out for each of the DEC-(H_2O)$_n$ heterodimers and also for the most stable heterotrimer, heterotetramer, and heteropentamer. Based on these energy values, the relative stabilities were determined. The isomeric population $\%X_i$ was calculated using Eq. (1):

$$\%X_i = \frac{g_i e^{-E_i/k_B T}}{\sum_i g_i e^{-E_i/k_B T}} \quad (1)$$

where g_i, is the degeneracy of the i^{th} isomer and k_B is the Bolztmann constant. T is the absolute temperature and E_i is the calculated energy of isomer i. Additionally, calculations of the energy decomposition analyses (EDA) proposed by Kitaura and Morokuma [47], and by Su and Li [48], were performed using GAMESS [34].

In order to study the geometric preferences of the DEC-(H_2O)$_n$ systems, the non-covalent intra- and intermolecular interactions obtained with both NCIPLOT [49] and AIMAll [50] (used in the free standard operating mode) codes were plotted. NCIPLOT is a program that enables the computation and graphical visualization of inter- and intramolecular non-covalent interactions via NCI, which is a visualization index based on the electron density (ρ) and the reduced density gradient. AIMAll is an implementation of algorithms that allow analysis of a wavefunction via the quantum theory of atoms in molecules (QTAIM) proposed by Bader et al. [50]. In addition to these wavefunction analysis methods, the evaluation of cooperative effects among O–H···O HBs was carried out through the analysis of differences in H···O and O···O distances, the red-shift of the stretching mode of the O–H bond at the proton donor molecule, and through the elongation of the O–H bonds in clusters in comparison to the isolated monomers.

Results and discussion

Diethyl carbonate conformers

In order to use the ASCEC-GAMESS interface to generate initial DEC-(H_2O)$_n$ geometries, a representative conformation is required. Thus, a detailed conformational analysis of the minimum energy conformations of DEC in the gas phase was carried out. A large group of DEC conformers was obtained from several MP2/6-311++G(d.p) bidimensional relaxed PES scans. An example of one such scan profile is shown in Fig. SM-1 in the electronic supplementary material (ESM). From the complete set of bidimensional relaxed PES scans, we found seven distinct stable DEC conformers (Fig. 1) along with their relative free energies with respect to the most stable DEC conformer (I): cis/trans–cis/trans [CC(TT)]. Free energies were obtained by the standard methods implemented in G09 [51]. Note that five DEC conformers have been already reported by Kar et al. [52] in their very recent experimental and theoretical study employing Ar matrix isolation infrared spectroscopy and electronic structure calculations at the B3LYP/6-31++G(d,p) level of theory. Highly correlated CCSD(T)/6-311++G(d,p) energy calculations on the MP2 geometries found herein confirm the same qualitative trends.

As an example of the method for naming these conformers, in the most stable DEC conformer: CC(TT), (I), both –CH_2– groups are cis-oriented with regard to the carbonyl group, and the –CH_3 terminal groups present opposed trans orientations forming a CCOC dihedral angle of 180°. The CC(TG) and CC(G+G−) DEC conformers are the closest in energy to the CC(TT) DEC conformer, which was also pointed out by Kar et al. [52] Additionally, the best agreement for the comparison of experimental infrared (IR) vibrational modes reported by Kar et al. [52] for the DEC conformer was found for the calculated CC(G+G−) DEC conformer in the present research at the MP2/6-311++G(d,p) level of theory (see Fig. SM-2). Therefore, for purposes of this investigation, the CC(G+G−) conformer (which is stabilized by intramolecular HBs) was used as the starting point to form the heteroclusters with water molecules, and subsequent optimization calculations were carried out without imposing any constraints on the system geometry.

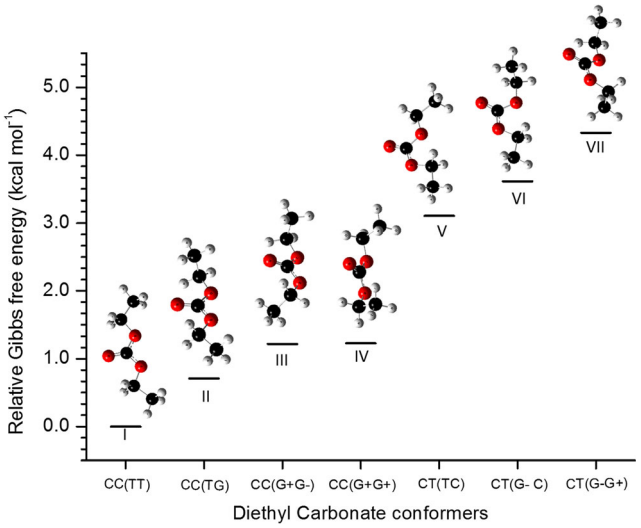

Fig. 1 Relative Gibbs energy (G = H − TS, T=298.15 K) of diethyl carbonate (DEC) conformers optimized with MP2/6-311++G(d,p). *I* {cis/trans – cis/trans} [0], *II* {cis/trans – cis/gauche)}[0.1], *III* {cis/gauche(+) – cis/gauche(−)}[0.2], *IV* {cis/gauche(+) – cis/gauche(+)}[0.18], *V* {cis/trans – trans/cis}[3.1] *VI* {cis/gauche(−) – trans/cis}[3.0], *VII* {cis/gauche(−) – trans/gauche (+)}[3.4]. The numbers in *brackets* are CCSD(T)/6-311++G(d,p)//MP2/6-311++G(d,p) values in kcal mol^{-1} at T=273.15 K

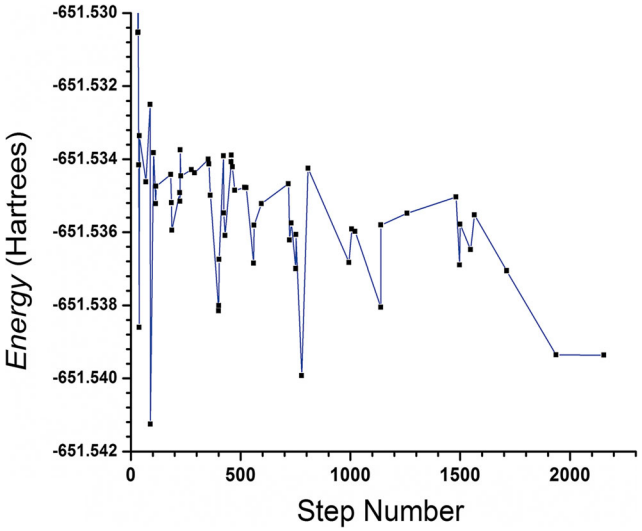

Fig. 2 Energy profile of the ASCEC-GAMESS run for DEC-$(H_2O)_2$ heterotrimers. Conditions: initial temperature: 500 K; temperature decrease: 5 %; number of temperatures: 100; cube length: 7 Å; and maximum cycles: 500 at each evaluated temperature. Level of theory: B3LYP/6-31+G(d)

Simulated annealing with quantum energy: ASCEC-GAMESS

Input geometries for DEC-$(H_2O)_n$ heteroclusters were generated by the Big Bang method implemented in the ASCEC code. An example of a typical energy profile (n=3) obtained by an ASCEC run is shown in Fig. 2.

In order to validate the programmed ASCEC-GAMESS interface, quite a few features can be highlighted from data plotted in Fig. 2 and Fig. SM-3 in the ESM. As examples, Fig. SM-3a,b show the energy of the candidate structures as a function of the temperature for the ASCEC runs of heterotrimers and heterotetramers. (1) The non-monotonic decrease of the energy shows the ability of the algorithm to jump over energy barriers on the PES (see Fig. 2); (2) most of the candidate structures are proposed at a low temperature range, between 280 and 370 K (see Fig. SM-3a); (3) the lowest energy candidate structure does not necessarily match the proposed structure at the lowest temperature of the simulation (see Fig. SM-3b). All these observations are consistent and reflect the behavior of the robust and efficient simulated annealing algorithm implemented in the ASCEC program as proposed by Pérez and Restrepo [33].

Geometries of DEC-$(H_2O)_n$, (n=1, 2, 3, 4) heteroclusters

Although B3LYP/6-31+G(d) showed 34 stable structures on the PESs for DEC-$(H_2O)_n$, n=1, 2, 3, and 4 heteroclusters (DEC(H_2O): 6, DEC$(H_2O)_2$: 9, DEC$(H_2O)_3$: 11, DEC$(H_2O)_4$: 8), further refinement at the MP2/6-311++G(d,p) level resulted in the location of only 22 true minima across all investigated values of n. Interestingly, these 22 minima keep the same geometrical motifs (defined as the arrangement of HBs and conformation of the DEC molecule) as DEC-$(H_2O)_n$, n=1, 2, 3, 4, heteroclusters found by B3LYP, differing only by small structural differences in the distances and angles. The 22 minima are classified as 3 heterodimers, 8 heterotrimers, 7 heterotetramers, and 4 heteropentamers. These heteroclusters are denoted Hdim_X, Htrim_X, Htet_X, and Hpen_X, where X is a number that indicates the stability order at each cluster size. For instance, X is 1, 2, or 3 for labeling the three heterodimers from the most to the least stable. All 22 MP2/6-311++G(d,p) heterocluster geometries are presented in Fig. 3 next to their respective relative energies with respect to the most stable structure and their isomeric populations at each cluster size. An interesting observation is that the DEC molecule may present a different conformation to the starting gas phase structure when solvated with water molecules. However, the DEC molecule conformations in the observed heterocluster all correspond to two of the most stable isolated DEC conformers: CC(TG) and CC(G+G−).

Some trends are easily identified for DEC-(H_2O) (i.e., n=1) heterodimers. For example, even at this smallest studied cluster size, two kinds of HBs are formed: O–H···O and C–H···O (hereafter, primary and secondary HBs, respectively). As is usually reported for other systems bound by HBs [30, 53, 54], the observed primary HBs are shorter than secondary HBs. Intermolecular HB distances for the most stable heterocluster at each cluster size are given in Fig. 3. In some cases, it has been

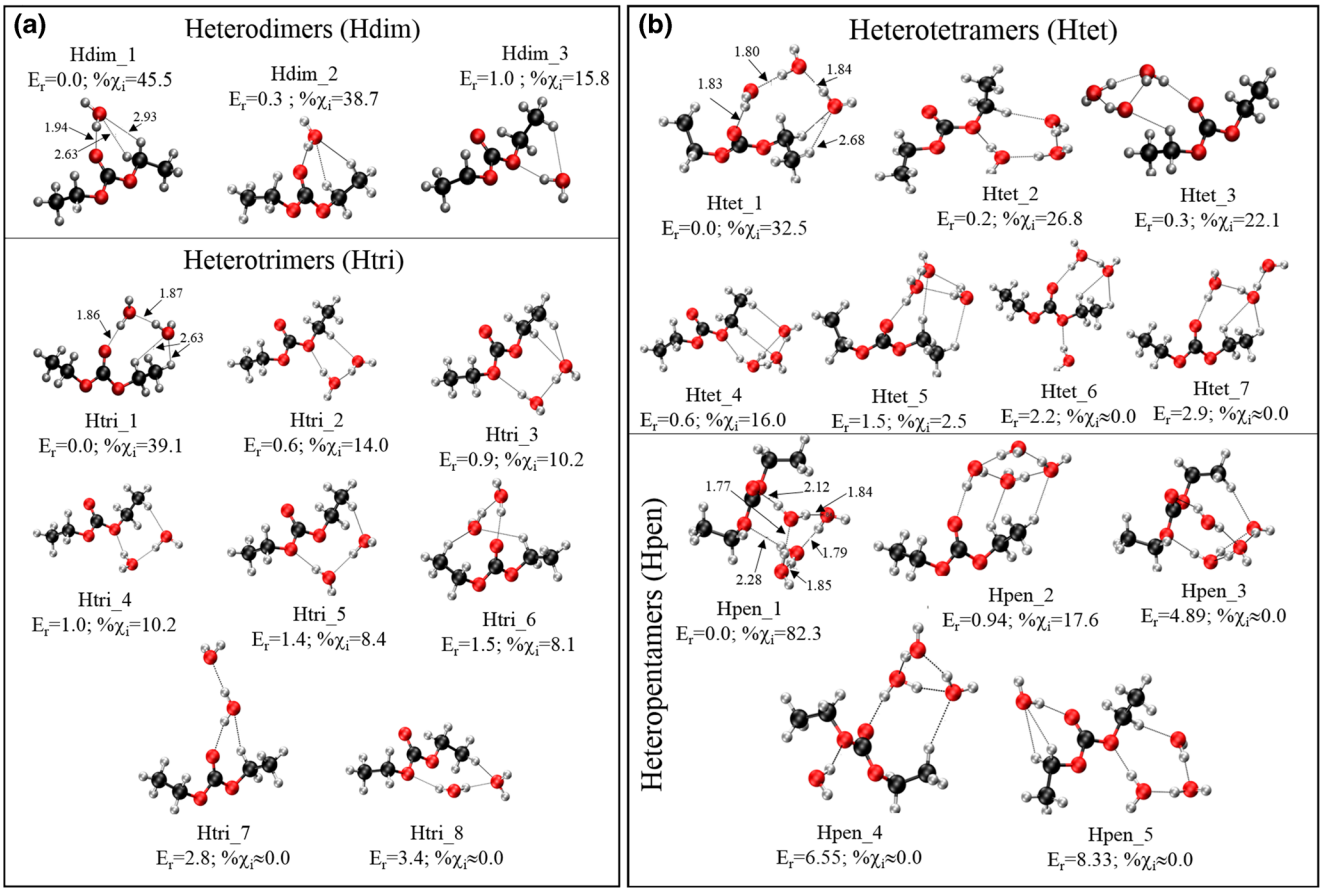

Fig. 3 **a** Optimized geometries of DEC-$(H_2O)_n$, n=1, 2, heteroclusters. Relative energy (E_r) in kcal mol^{-1} corrected with the counterpoise method besides the vibrational zero point energy (ZPE). Isomeric population (%χ_i). MP2/6-311++G(d,p). Intermolecular hydrogen bond (HB) distances for the most stable heterocluster at each cluster size. **b** Optimized geometries of DEC-$(H_2O)_n$, n=3, 4, heteroclusters. Relative energy (E_r) in kcal mol^{-1} corrected with the counterpoise method besides the vibrational ZPE. Isomeric population (%χ_i). MP2/6-311++G(d,p). Intermolecular HB distances for the most stable heterocluster at each cluster size

found that structures that present both these kinds of HBs present atypically strong secondary HBs compared with their primary HBs. This unusual observation has been explained as being due (among other reasons) to the phase of the calculations, i.e., condensed phase rather than gas phase [20, 55]. Focusing on the most stable heteroclusters at each cluster size, we observe that the water molecule interacting by primary HBs with the DEC molecule prefers the oxygen atom of the DEC carbonyl group as the proton acceptor rather than one of the alkoxy oxygen atoms. As expected, a higher atomic charge is concentrated at the oxygen atom of the carbonyl group (average Mulliken atom charge: −0.420 e) than the atomic charge on the oxygen atoms of the ethoxy group (average Mulliken atom charge: −0.170 e). This favors the carbonyl oxygen when determining which site is a good proton acceptor. Mulliken atomic charges for the most stable heteroclusters at each cluster size are shown in Fig. 4. It was also observed that Htri_7 and Htri_8 are the least stable and probable heterotrimers, and both are characterized by a water molecule acting as double proton donor in two primary HBs. Heterotetramers with water molecules forming a cyclic substructure amongst themselves are not favored as much as the case where the maximum number of water molecules act simultaneously as proton donor and acceptor in primary HBs. This trend is not followed when the number of water molecules increases from 3 to 4 due to the fact that a stable heteropentamer where the three of the four water molecules act only as proton donor and acceptor at the same time in primary HBs was not found. This is in accordance with the presence of cooperative effects among primary HBs (see section on Cooperative effects). It has been observed that primary HBs where a molecule acts as proton double donor or double acceptor are mutually weakened [19, 22].

Energy analysis

Highly correlated energies [CCSD(T)/6-311++G(d,p)] for the optimized geometries at the MP2/6-311++G(d,p) level were calculated for the most stable DEC-$(H_2O)_n$ heteroclusters, and are listed in Table 1. The stability order at the MP2 level was maintained after refining the energies with CCSD(T).

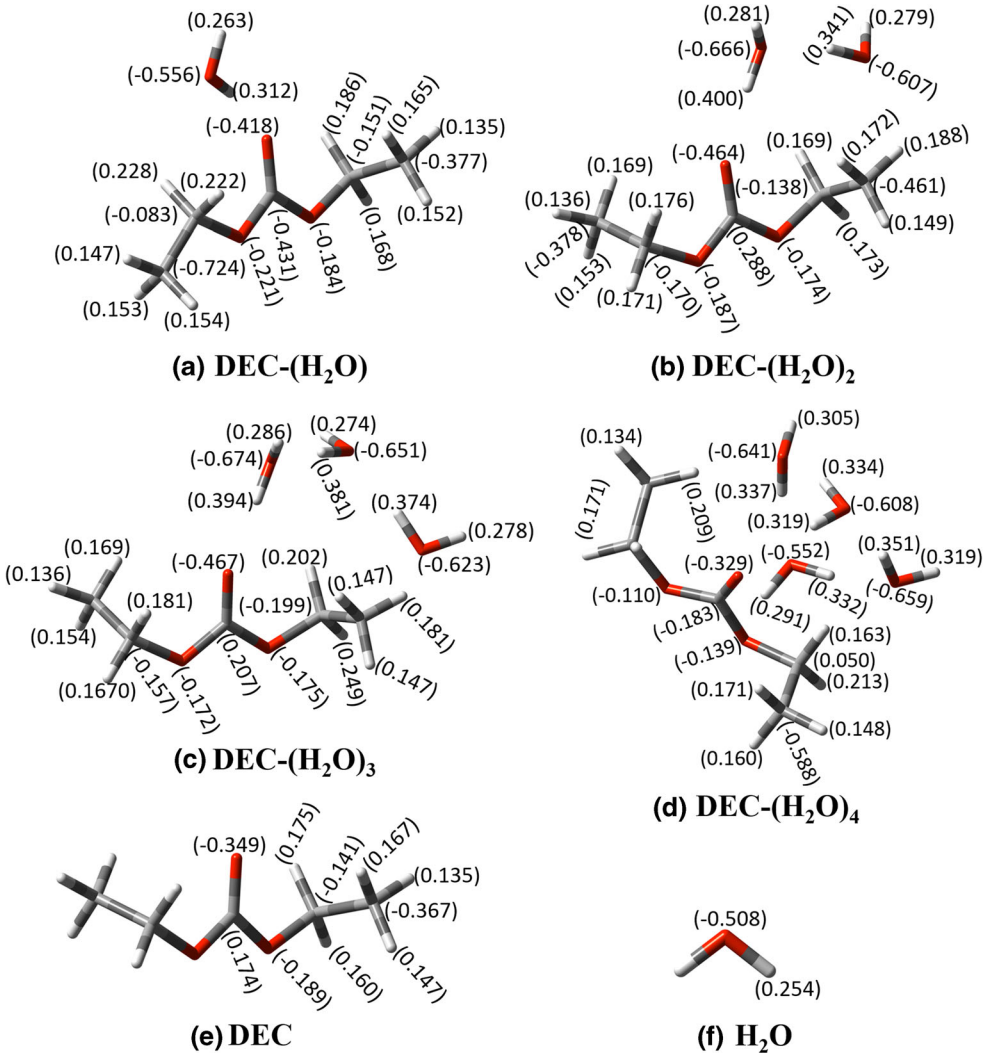

Fig. 4a–f Mulliken atomic charges (units: e). **a**, **b**, **c**, **d** Most stable DEC-$(H_2O)_n$, n=1, 2, 3, 4, heteroclusters. **e** Isolated water molecule. **f** CC(G+G−) Isolated DEC conformer. MP2/6-311++G(d,p)

Deviations lower than 5.3 % for the interaction energies show the suitability of our MP2 results for detailed analysis. In general, the more primary HBs formed, the more stable the heteroclusters. However, an interesting conclusion is obtained when the stabilization energy per primary HB is considered. Primary HBs become stronger when the heterocluster has more than one interaction of that kind until a fourth water molecule participates. For the Hpen_1 conformation, the $\Delta E/\#HB$ value is smaller than the corresponding value for the Hdim_1 conformation. These results indicate that non-covalent interactions are affected by cooperative effects, as discussed below.

Table 1 Interaction energy and interaction energy per O–H···O HB in kcal mol^{-1} for the most stable (DEC)-$(H_2O)_n$, n=1, 2, 3, and 4, heteroclusters. Basis set: 6-311++G(d,p)

n	CCSD(T)[a]		MP2		%Deviation[b]
	$\Delta E_{CCSD(T)}$	$\Delta E_{CCSD(T)}/\#HB$	ΔE_{MP2}	$\Delta E_{MP2}/\#HB$	
1	−7.03	−7.03	−7.03	−7.03	0.00
2	−16.24	−8.12	−16.10	−8.05	0.86
3	−24.34	−8.11	−25.64	−8.55	5.34
4	−40.35	−6.72	−40.25	−6.71	0.24

[a] Values obtained from single point energy calculations at CCSD/6-311++G(d,p) level for the optimized structures at MP2/6-311++G(d,p)

[b] %Deviation=$|\Delta E_{MP2}-\Delta E_{CCSD(T)}|/\Delta E_{CCSD(T)}*100$

Furthermore, while the most stable structure at each cluster size corresponds to the structure with the highest isomeric population: Hdim_1: 46 %, Htrim_1: 39 %, Htet_1: 32 %, and Hpen_1: 82.3 %, the isomeric populations remain significant (>10 %) for even the fourth most stable structures of the heterotrimers and heterotetramers (see Fig. 3). This suggests that their energy contributions must be taken into account for a suitable understanding of the stability of the DEC-water system. For this reason, the energy analysis in this section includes all heteroclusters optimized at each cluster size.

Energy decomposition analysis

The EDA proposed by Hashimoto and Morokuma [47] was employed to analyze the stability of DEC-$(H_2O)_n$ heteroclusters, paying attention mainly to the effect of increasing the number of water molecules present. In this scheme, the total binding energy is separated into solvent–solvent and solute–solvent contributions, as in Eqs. (2) and (3), respectively.

Interaction energy of H_2O–H_2O $\left(\Delta E_{(H_2O-H_2O)}\right)$:

$$\Delta E_{(H_2O-H_2O)} = \left[E(H_2O)_n^* - nE(H_2O)\right] \quad (2)$$

Interaction energy of DEC–H_2O (ΔE_{DEC-H_2O}):

$$\Delta E_{(DEC-H_2O)} = \left[E\left(DEC-(H_2O)_n\right) - E(DEC) - E(H_2O)_n^*\right] \quad (3)$$

Where $E(H_2O)_n{}^*$ is the energy associated with the supermolecule formed by n water molecules at the respective DEC$-(H_2O)_n$ heterocluster geometry, $\Delta E_{(H_2O-H_2O)}$ is defined as the interaction energy of the solvent molecules in the heterocluster, and $\Delta E_{(DEC-H_2O)}$ is the interaction energy between the supermolecule formed from the DEC and the solvent molecules.

The sum of these two energies is the binding energy (ΔE_B), Eq. (4):

$$\Delta E_B = \Delta E_{(H_2O-H_2O)} + \Delta E_{(DEC-H_2O)} \quad (4)$$

The energy contributions, ΔE_B, $\Delta E_{(DEC-H_2O)}$, and $\Delta E_{(H_2O-H_2O)}$ are shown in Table 2. Firstly, we note that all interactions in the DEC-H_2O heteroclusters are stabilizing (negative values).

It is worth highlighting that the binding energies for DEC-$(H_2O)_n$ (16–40 kcal mol^{-1}) are bigger than the corresponding energies for the most stable water clusters with the same geometric pattern (dimer = −6.0 kcal mol^{-1}, trimer = −17.5 kcal mol^{-1}, tetramer = −30.5 kcal mol^{-1}) [37] at the CCSD(T)/6-311++G(d,p)//MP2/6-311++G(d,p) level of theory, revealing a strengthening due specifically to the presence of the DEC molecule.

Remarkably, the most stable heteropentamer does not follow the trend observed by the most stable heteroclusters. Specifically, the $\Delta E_{(DEC-H_2O)}$ interaction energy for Hpen_1 is smaller than that calculated for the most stable heterotetramer (Htet_1), while its value of $\Delta E_{(H_2O-H_2O)}$ is more than twice as high as the corresponding value for Htet_1. Therefore, the DEC molecule interacts more strongly with three water molecules than it does with four water molecules.

Table 2 EDA of Hashimoto and Morokuma for DEC-$(H_2O)_n$, n=1, 2, 3, and 4, heteroclusters. Total binding energy, ΔE_B, solute–solvent, $\Delta E_{(DEC-H_2O)}$, and solvent–solvent, $\Delta E_{(H_2O-H_2O)}$, interactions are in (kcal mol^{-1}). MP2/6-311++G(d,p)

Heterocluster	$\Delta E_{(H_2O-H_2O)}$	$\Delta E_{(DEC-H_2O)}$	ΔE_B
DEC-H_2O			
Hdim_1	–	−6.37	−6.37
Hdim_2	–	−6.96	−6.96
Hdim_3	–	−6.93	−6.93
DEC-$(H_2O)_2$			
Htri_1	−5.78	−10.63	−16.40
Htri_2	−5.73	−9.95	−15.68
Htri_3	−5.63	−10.03	−15.66
Htri_4	−6.26	−9.23	−15.49
Htri_5	−5.23	−10.86	−16.09
Htri_6	−5.79	−5.85	−11.64
Htri_7	−5.77	−9.75	−15.52
Htri_8	−6.02	−6.04	−12.06
DEC-$(H_2O)_3$			
Htet_1	−12.72	−14.20	−26.92
Htet_2	−13.82	−11.80	−25.62
Htet_3	−17.29	−8.27	−25.56
Htet_4	−16.90	−8.45	−25.34
Htet_5	−11.59	−12.94	−24.53
Htet_6	−5.12	−16.78	−21.90
Htet_7	−10.51	−10.75	−21.26
DEC-$(H_2O)_4$			
Hpen_1	−29.64	−10.97	−40.61
Hpen_2	−29.82	−9.44	−39.26
Hpen_3	−22.27	−12.48	−34.75
Hpen_5	−13.97	−18.38	−32.35
Hpen_4	−16.96	−15.12	−32.08

In addition to the Hashimoto/Morokuma scheme, the EDA proposed by Su and Li [48] was also employed to understand the nature of the energy contributions at both interaction energies: $\Delta E_{(DEC-H_2O)}$ and $\Delta E_{(H_2O-H_2O)}$. In this scheme, those interaction energies are divided into terms corresponding to electrostatic energy (ΔE^{Elec}), repulsion (ΔE^{Rep}), exchange (ΔE^{Exc}), polarization + charge transfer (ΔE^{pol+ct}) and finally a dispersion (ΔE^{disp}) term calculated by a post-HF correction to the interaction energy. The energy decomposition for the DEC-H_2O (Ste) interaction energy for all heteroclusters is described in Table SM-1 of the ESM. The electrostatic energy (ΔE_{Ste}^{Elec}), exchange energy (ΔE_{Ste}^{Exc}) and the polarization and charge transfer energy (ΔE_{Ste}^{pol+ct}) are always negative (stabilizing) for all DEC-H_2O heteroclusters. The dispersion energy (ΔE_{Ste}^{Disp}) is negative only for the heterodimers. For the rest of the heteroclusters, dispersion (ΔE_{Ste}^{Disp}) and repulsion (ΔE_{Ste}^{Rep}) are destabilizing (positive valued) energies. Regarding

magnitude, the stabilizing terms, ΔE_{Ste}^{Elec} and ΔE_{Ste}^{Intc} contribute on average 4 and 3 times more than the ΔE_{Ste}^{pol+ct} term respectively. Particularly, for the most stable heteropentamer, the destabilizing ΔE_{Ste}^{Rep} term proved to be up to 75 times higher than the ΔE_{Ste}^{Disp} term. See the graphic of these values for the most stable DEC-$(H_2O)_n$, n=1, 2, 3, and 4, heteroclusters in Fig. 5.

In Fig. 5, a balance is observed between ΔE_{Ste}^{Elec}, ΔE_{Ste}^{Intc} and the ΔE_{Ste}^{Rep} interaction energies. For example, the electrostatic and exchange energy contributions stabilize the heterotetramer around 80 kcal mol^{-1} in comparison with the heterodimer. The ΔE_{Ste}^{pol+tc} term is small by comparison, being responsible for around 11 kcal mol^{-1} of the stabilization of that heterotetramer. The increase in stabilizing contributions from the heterotetramer to the heteropentamer is almost 3 times less than that increase observed from the heterotrimer to the heterotetramer.

Similarly, the energy decomposition for the H_2O–H_2O (Snt) interaction energy for all heteroclusters is described in Table SM-2 of the ESM. The polarization and charge transfer energy (ΔE_{Snt}^{pol+ct}) contributes five times less to the stabilization of the supermolecule formed by n water molecules than the ΔE_{Snt}^{Elec} and ΔE_{Snt}^{Exc} terms, which have mutually similar magnitudes. The main destabilizing factor is the repulsion energy (ΔE_{Snt}^{Rep}). Information presented in Fig. 6 shows that electrostatic and exchange interactions are the biggest contributors to the total for all water supermolecules. For instance, on going from two to three water molecules, there is an increase in stabilization of 44 kcal mol^{-1} due to the ΔE_{Snt}^{Elec} and ΔE_{Snt}^{Int} terms. Whereas on going from three to four water molecules, the increase in the stabilization is 18 % of the previous value

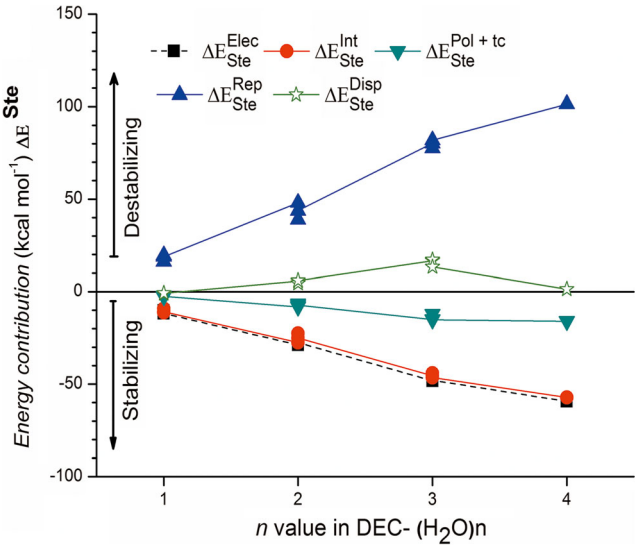

Fig. 5 EDA proposed by Su and Li for solute–solvent DEC-H_2O (Ste) interaction terms. Values for the most stable DEC-H_2O heteroclusters with equal geometric pattern for the HBs. *Elec* Electrostatic, *Exc* exchange, *Rep* repulsion, *Pol+ct* polarization and charge transfer, *Disp* dispersion. Level of theory: MP2/6-311++G(d,p), values in kcal mol^{-1}

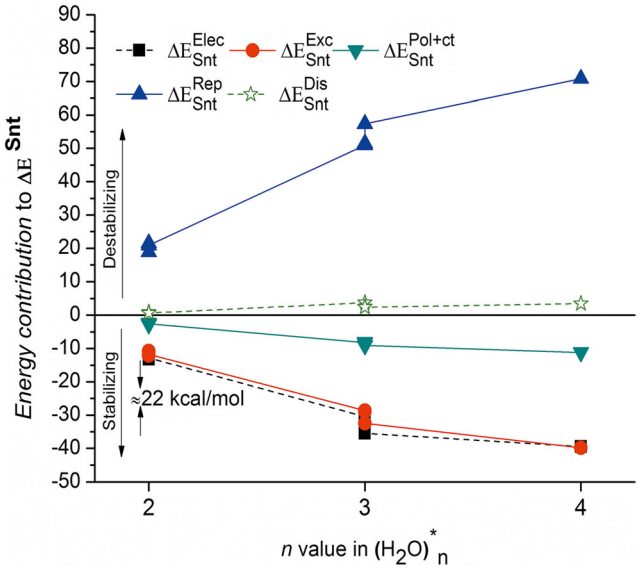

Fig. 6 EDA proposed by Su and Li for H_2O–H_2O (Snt) interaction terms. Values for the most stable DEC-H_2O heteroclusters with an equal geometric pattern of HBs. *Elec* Electrostatic, *Exc* exchange, *Rep* repulsion, *Pol+ct* polarization and charge transfer, *Disp* dispersion. Level of theory: MP2/6-311++G(d,p), values in kcal mol^{-1}

(~8 kcal mol^{-1}). These behaviors are associated with structural changes in the water supermolecule as n increases. The relative magnitudes of the ΔE_{Snt}^{Elec} and ΔE_{Snt}^{Exc} terms compared to the other terms supports that these forces determine the stability of the heteroclusters, which in turn is associated with the formation of HBs [56–58]. The next section provides an analysis of the characterization of intermolecular interactions based on NCI and AIM analysis.

Non-covalent interactions in DEC-$(H_2O)_n$ heteroclusters

The HBs of the heteroclusters were revealed by NCI analysis [49, 59]. In NCI methodology the reduced density gradient, S, is defined according to Eq. (5):

$$S = \frac{1}{2(3\pi^2)^{1/3}} \frac{|\nabla\rho|}{\rho^{4/3}} \tag{5}$$

where ρ is the electron density. When an intermolecular or intramolecular interaction is formed, there is an accompanying noticeable change in the reduced density gradient between the interacting atoms. This change generates critical points of the molecular electron density between the interacting fragments. The electron density values at these critical points are an indicator of the interaction strength. Both attractive and repulsive interactions appear in the same space region, ρ/S. However, the Laplacian of the electron density, $\nabla^2\rho$, and the λ_2 eigenvalue of the Hessian matrix, which can be positive or negative, can be used as an indicator of interaction type. Thus, bonding interactions, such as strong HBs, are characterized by an accumulation of electron density perpendicular to the bond

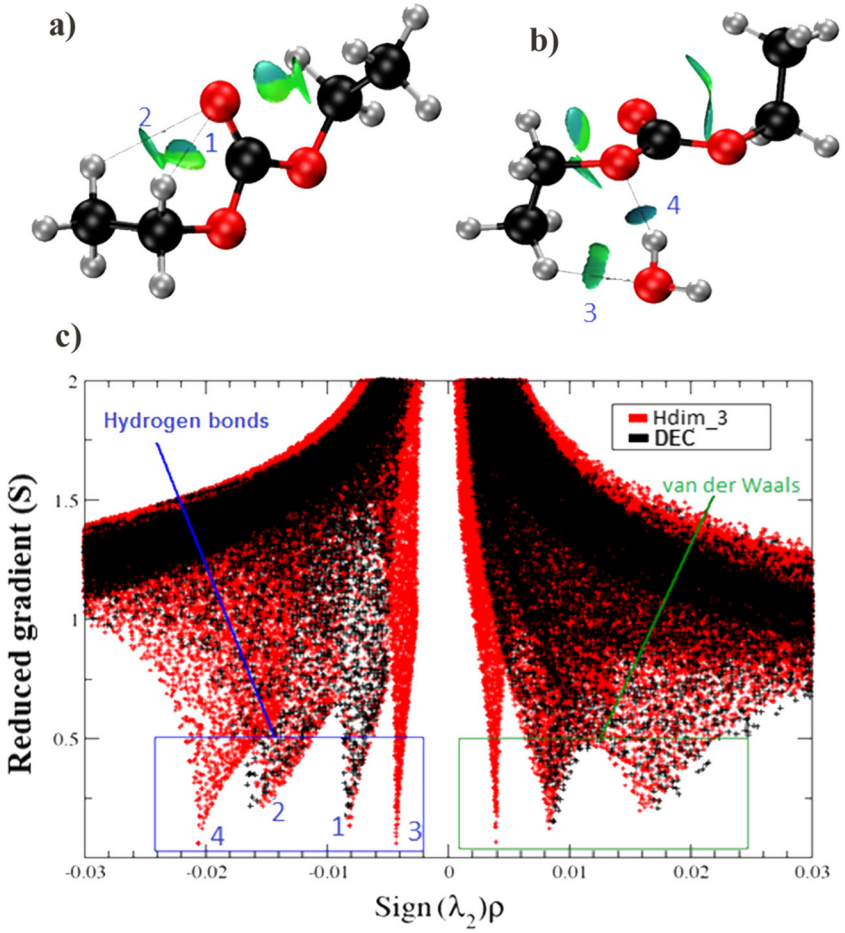

Fig. 7a–c Non-covalent interaction (NCI) isosurfaces [MP2/6-311++G(d,p)]. **a** DEC conformer [CC(G+G−)]. **b** DEC-H_2O heterodimer (Hdim_3). **c** Overlaid graphics of the reduced density gradient (S=0.5 au) versus $sign(\lambda_2)\rho$. −0.03 au < ρ < + 0.03 au

line and so $\lambda_2<0$. In contrast, non-bonding interactions such as steric repulsions cause a decrease in the electron density with $\lambda_2>0$. Finally, the van der Waals type of interaction is characterized by a small, positive electron density with $\lambda_2\approx0$.

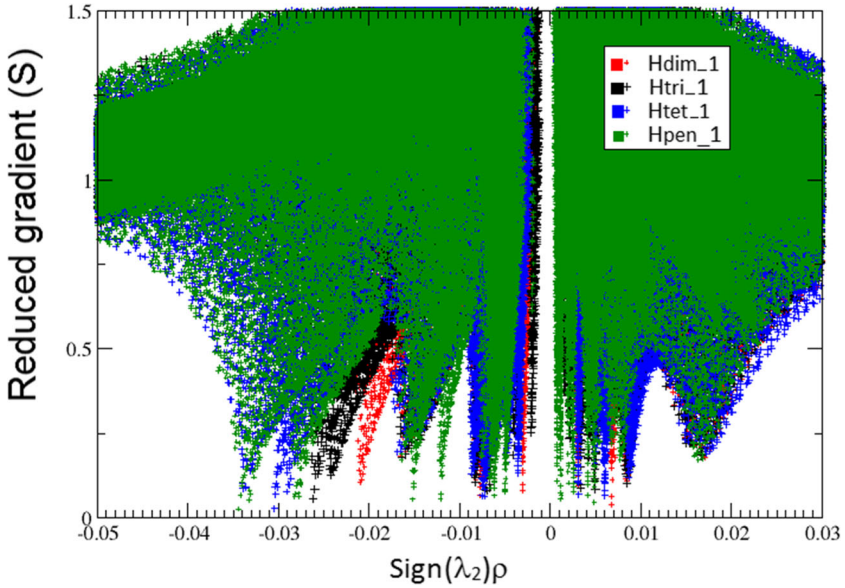

Fig. 8 Overlaid graphics of the reduced density gradient (S=0.5 au) vs the $sign(\lambda_2)\rho$ (-0.03 au < ρ < +0.03 au). Structures: the most stable DEC-$(H_2O)_n$, n=1, 2, 3, and 4, heteroclusters. MP2/6-311++G(d,p)

Considering NCI methodology, as an example, a plot of the dependence of S on the $sign(\lambda_2)\rho$ is shown in Fig. 7. Figure 7a,b correspond to three-dimensional (3D) isosurfaces of non-covalent interactions for the CC(G+G−) DEC conformer and the Hdim_3 heterocluster, respectively. Hdim_3 was chosen because of its simplicity. It is stabilized by two HBs: one primary and one secondary. These results show asymmetrical and polarized isosurfaces. This suggests that the geometric stability of the most stable DEC conformer is due to intramolecular HBs that have different contributions (stabilizing, blue section on the isosurface) besides certain repulsive character (green section on the isosurface).

When a water molecule interacts with the DEC molecule, new isosurfaces appear (see Fig. 7b). On one hand, the blue disc indicates a very localized interaction according to the NCI scheme [59]. On the other hand, a secondary HB is evidenced by the green isosurface (weak type). According to NCI classification, this green isosurface corresponds to an interaction of the van der Waals type. It implies a HB with highly dispersive character in comparison to the primary HB with highly electrostatic character. To support this observation, several minima of the 2D NCI plots are given for the DEC conformer and Hdim_3 shown in Fig. 7c. The negative region of the abscissa shows attractive interactions such as the primary HBs, for instance the minimum 4. This interaction is around eight times stronger than the secondary HB (minimum 3). It is worth noting that the intramolecular secondary HB (minimum 1) is stronger than the same kind of HB, minimum 3, which is an intermolecular interaction. At the positive region of $sign(\lambda_2)\rho$, there are several bands corresponding to repulsive interactions. Therefore, the strength order for the HBs of the DEC-water system is: O–H···O > C–H···O (intramolecular) > C–H···O (intermolecular).

The complete set of 3D NCI plots for the most stable DEC-$(H_2O)_n$ heteroclusters are gathered in Fig. SM-4 of the ESM. The most stable heteropentamer is characterized because all water molecules form a cyclic pattern via primary HBs. As expected, these HBs are manifested by blue isosurfaces. Therefore, the water molecules interacting via quite strong stabilizing interactions and, remarkably, the primary HB between the water molecule and the DEC molecule shows a high repulsive character as represented by the green color of the isosurface. This result suggests an explanation for the 1:3 experimental relationship found by Arango and Villa [15] for the DEC-H_2O azeotrope. If the relationship for DEC:H_2O is higher, for instance 1:4, our results suggest that the most stable structure reported in this study for that heteropentamer reveals a high repulsive character for the DEC-H_2O intermolecular interactions representing a weaker set of interactions than those observed for the most stable DEC-$(H_2O)_3$ heterotetramer.

To generalize this result, the HB strength involved in each of the most stable DEC-$(H_2O)_n$ heteroclusters with respect to the water molecules were compared. Figure 8 shows a plot of overlaid graphics of the reduced density gradient versus the $sign(\lambda_2)\rho$ for these heteroclusters. It is seen that at the $-0.032 < sign(\lambda_2)\rho < -0.021$ region, the strength order: blue > green > black > red, indicates that the interaction strength decreases as

Table 3 Cooperative effect indices for the most stable DEC-$(H_2O)_n$, n=1, 2, 3, and 4, heteroclusters. HB, d_HB, and O···O, d(O···O), distances, O–H bond elongation, Δr(O–H), and the red-shift of its stretching frequency, Δν(O–H), at the proton donor molecule and the cooperative factor, A_b

n	d_HB (Å)	d(O···O) (Å)	Δr(O-H) (Å)	Δν(O–H) (cm^{-1})	A_b
Scheme 1					
1	1.945	2.897	0.007	94.5	1.00
2	1.864	2.833	0.011	137.5	1.45
3	1.829	2.799	0.012	170.7	1.81
4	2.118	3.001	0.006	25.2	0.27
Scheme 2					
1	1.975	2.887	0.006	129.5	1.00
2	1.933	2.857	0.009	166.3	1.28
3	1.889	2.855	0.010	197.6	1.53
4	2.278	3.075	0.004	133.2	1.02

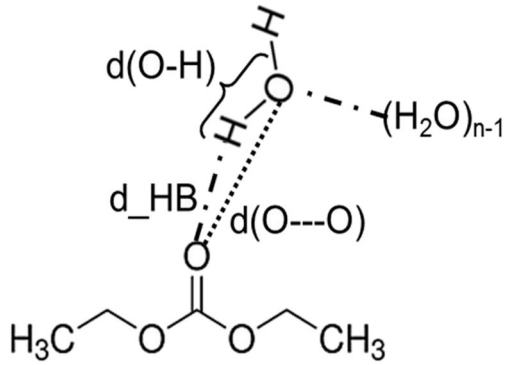

Scheme 1 Specification of the geometric data employed as cooperative effect indices for the primary hydrogen bond (HB) formed between a water molecule and the oxygen atom of the carbonyl group at the diethyl carbonate (DEC) molecule

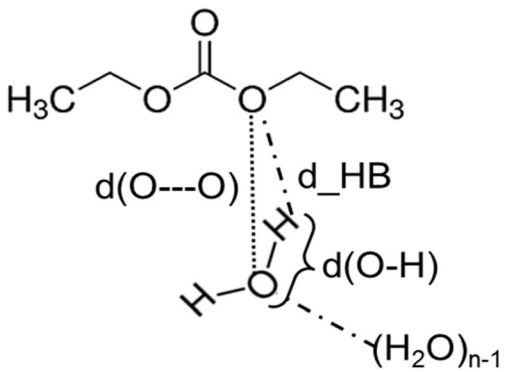

Scheme 2 Specification of the geometric data employed as cooperative effect indices for the primary HB formed between a water molecule and one alkoxy oxygen of the DEC molecule

follows: DEC-$(H_2O)_3$ > DEC-$(H_2O)_4$ > DEC-$(H_2O)_2$ > DEC-(H_2O). Similarly, the secondary HB region [$-0.01 < sign(\lambda_2)\rho < 0.0$] shows stronger interactions (blue band) in Htet_1 compared with Hpen_1 (green band). These observations motivate an a posteriori analysis of the cooperative effects among those interactions (see Cooperative effects).

Finally, the NCI and the AIM results predict in general the same trends. For example, bond critical point positions match the NCI isosurface positions for intermolecular interactions. Figure SM-4 shows a comparison of molecular graphs of the most stable DEC-$(H_2O)_n$ heteroclusters with their respective 3D isosurfaces of non-covalent interactions. However, several intramolecular HBs revealed by the NCI methodology were not observed in the AIM results. This difference has been found in other systems bounded by HBs, such as 2-aminoethanol and 3-aminopropanol. Thomsen et al. [60] found evidence of HB formation in their gas-phase vibrational spectra that in both molecules were supported by NCI analysis, while the AIM analysis supported only the 3-aminopropanol result.

Cooperative effects

How multiple HBs affect each other can be studied by analysis of their cooperative effects. Some data, such as geometric and spectroscopic data, can be used as cooperative indices. In this particular study, we analyzed changes with respect to n in the O···O and HB distances, as well as the elongation of O–H bonds of the proton donor molecules (H_2O for these heteroclusters) and therefore the red-shift of their stretching frequencies when more than one primary HB is formed. The cooperative factor, A_b, was also analyzed. This factor relates the redshift of the donor O–H stretch in the heterocluster [$\Delta\nu$(O–H)] to the corresponding redshift in the heterodimer [$\Delta\nu$'(O–H)] for each O–H···O HB A_b=[$\Delta\nu$(O–H)]/[$\Delta\nu$'(O–H)]. As an example, these data are collected in Table 3 for the most stable heteroclusters at each cluster size for both cases: primary HBs with the oxygen atom of the carbonyl group (Scheme 1) and with one alkoxy oxygen of the DEC molecule (Scheme 2).

It should be noted that, when increasing the number of water molecules, primary HBs with the oxygen atom of the carbonyl group show the following changes in characteristics: the O···O distances become longer, Δr(O–H) and $\Delta\nu_d$ increase as well as the cooperative factor while d_HB distances become shorter. Values greater than 1 for A_b indicate the existence of positive cooperative effects. This behavior is present when three or fewer water molecules are present in the heterocluster. When a fourth water molecule is added to the heterocluster, an increase of the d_HB distance is observed as well as an elongation of the O–H bond even smaller than the one observed for the heterodimer. In addition, the red-shift is reduced drastically and the cooperative factor is less than 1. This indicates a weakening of the primary HB. Similar trends are evidenced for the primary HBs illustrated in Scheme 2. Upon reaching four water molecules, the HB and O···O distances increase instead of decreasing, the red-shift decreases and the cooperative factor is barely of unit value. Hence, this type of result also agrees that the interactions of the DEC molecule with water molecules are favored until a 1:3 ratio of DEC-H_2O is reached, in accordance with experimental data.

Conclusions

Twenty-two stable geometries were found for DEC-$(H_2O)_n$, n=1, 2, 3, and 4 heteroclusters by a configurational exploration of the respective PES with B3LYP/6-31+G(d) and a subsequent optimization and characterization with MP2/6-311++G(d,p). The fitness of the MP2 level for describing the energetics of the DEC-$(H_2O)_n$ systems was confirmed by energy calculations at CCSD(T)/6-311++G(d,p) on the MP2 structures. The stabilization of DEC-$(H_2O)_n$ heteroclusters is associated with the number of O–H···O HBs but also with the cooperative effects amongst those mainly electrostatic interactions, while secondary HBs present higher dispersive contributions. Intramolecular interactions of the DEC molecule (secondary HBs) are stronger than the secondary HBs formed amongst the DEC molecule and water molecules, although both kinds of interactions are weaker than the primary HBs. A comparison of the solute-solvent interactions via energy partitioning analysis of the most stable structures shows that the strongest interaction between the water molecules and the DEC molecule is in the heterotetramer rather than the heteropentamer. This observation was supported by the rest of the analyses made. Thus, NCI and AIM analyses and different data employed as cooperative indices confirm that the heteropentamer shows a weakened primary HB that binds the water molecules cluster to the DEC molecule in comparison with the heterotetramer. These results at molecular level suggest an explanation for the 1:3 molar relation found experimentally for the DEC-H_2O azeotrope.

Acknowledgments The authors would like to thank the Universidad de Antioquia (Sustainability Strategy 2013-2014) and the Pontifica Universidad Javeriana for financial support of this work. J.D.R. thanks "Colciencias" and the Universidad de Antioquia for his PhD scholarship. Additionally, great gratitude is due to Professor Albeiro Restrepo for permission to use the ASCEC program.

References

1. Peters GP, Marland G, Le Quéré C, Boden T, Canadell JG, Raupach MR (2012) Rapid growth in CO_2 emissions after the 2008–2009 global financial crisis. Nat Clim Chang 2:2–4. doi:10.1038/nclimate1332
2. Patz J, Gibbs H, Foley J, Rogers J, Smith K (2007) Climate change and global health: quantifying a growing ethical crisis. EcoHealth 4(4):397–405. doi:10.1007/s10393-007-0141-1

3. Dias De Oliveira ME, Vaughan BE, Rykiel EJ (2005) Ethanol as fuel: energy, carbon dioxide balances, and ecological footprint. Bioscience 55(7):593–602. doi:10.1641/0006-3568(2005)055[0593:eafecd]2.0.co;2
4. Watson JG, Chow JC, Fujita EM (2001) Review of volatile organic compound source apportionment by chemical mass balance. Atmos Environ 35(9):1567–1584. doi:10.1016/S1352-2310(00)00461-1
5. Gee IL, Sollars CJ (1998) Ambient air levels of volatile organic compounds in Latin American and Asian cities. Chemosphere 36(11):2497–2506. doi:10.1016/S0045-6535(97)10217-X
6. Perry R, Gee IL (1995) Vehicle emissions in relation to fuel composition. Sci Total Environ 169(1–3):149–156. doi:10.1016/0048-9697(95)04643-F
7. Balasubramaniyan K, Balashanmugam P, Raghupathy A, Balasubramanian G (2013) Studies on emission characteristics of diesel engine run using diesel di methoxy ethane blend fuel. Int J Sci Eng Technol Res 2(11):2031–2037
8. Mendonca S, Vas JP (2013) Effect of oxygenated fuel additive on dibutyl ether on diesel engine. Int J Sci Res Publ 3(4):1–6
9. Senthil R, Kannan M, Deepanraj B, Nadanakumar V, Santhanakrishnan S, Lawrence P (2011) Study on performance and emission characteristics of a compression ignition engine fueled with diesel-2 ethoxy ethyl acetate blends. Engineering 3(11):1132–1136. doi:10.4236/eng.2011.311141
10. Pacheco MA, Marshall CL (1997) Review of dimethyl carbonate (DMC) manufacture and its characteristics as a fuel additive. Energy Fuel 11(1):2–29. doi:10.1021/ef9600974
11. Lapuerta M, Armas O, Rodríguez-Fernández J (2008) Effect of biodiesel fuels on diesel engine emissions. Prog Energy Combust Sci 34(2):198–223. doi:10.1016/j.pecs.2007.07.001
12. Arbeláez O, Orrego A, Bustamante F, Villa A (2012) Direct synthesis of diethyl carbonate from CO_2 and CH_3CH_2OH over Cu–Ni/AC catalyst. Top Catal 55(7–10):668–672. doi:10.1007/s11244-012-9849-4
13. Arteconi A, Mazzarini A, Nicola G (2011) Emissions from ethers and organic carbonate fuel additives: a review. Water Air Soil Pollut 221(1–4):405–423. doi:10.1007/s11270-011-0804-y
14. Roh N-S, Dunn BC, Eyring EM, Pugmire RJ, Meuzelaar HLC (2003) Production of diethyl carbonate from ethanol and carbon monoxide over a heterogeneous catalytic flow reactor. Fuel Process Technol 83(1–3):27–38. doi:10.1016/S0378-3820(03)00079-1
15. Arango IC, Villa AL (2013) Isothermal vapor–liquid and vapor–liquid–liquid equilibrium for the ternary system ethanol + water + diethyl carbonate and constituent binary systems at different temperatures. Fluid Phase Equilib 339:31–39. doi:10.1016/j.fluid.2012.11.026
16. Uragami T, Katayama T, Miyata T, Tamura H, Shiraiwa T, Higuchi A (2004) Dehydration of an ethanol/water azeotrope by novel organic–inorganic hybrid membranes based on quaternized chitosan and tetraethoxysilane. Biomacromolecules 5(4):1567–1574. doi:10.1021/bm0498880
17. Al-Amer AM (2000) Investigating polymeric entrainers for azeotropic distillation of the ethanol/water and MTBE/methanol systems. Ind Eng Chem Res 39(10):3901–3906. doi:10.1021/ie0000515
18. de Lima GF, Mavrandonakis A, de Abreu HA, Duarte HA, Heine T (2013) Mechanism of alcohol–water separation in metal–organic frameworks. J Phys Chem C 117(8):4124–4130. doi:10.1021/jp312323b
19. Mejía SM, Flórez E, Mondragón F (2012) An orbital and electron density analysis of weak interactions in ethanol-water, methanol-water, ethanol and methanol small clusters. J Chem Phys 136(14):144306. doi:10.1063/1.3701563
20. Mejía SM, Orrego JF, Espinal JF, Fuentealba P, Mondragón F (2011) Exploration of the $(ethanol)_4$–water heteropentamers potential energy surface by simulated annealing and ab initio molecular dynamics. Int J Quantum Chem 111(12):3080–3096. doi:10.1002/qua.22664
21. Nedic M, Wassermann TN, Larsen RW, Suhm MA (2011) A combined Raman- and infrared jet study of mixed methanol-water and ethanol-water clusters. Phys Chem Chem Phys 13(31):14050–14063. doi:10.1039/C1CP20182D
22. Mejía SM, Mills MJL, Shaik MS, Mondragóon F, Popelier PLA (2011) The dynamic behavior of a liquid ethanol-water mixture: a perspective from quantum chemical topology. Phys Chem Chem Phys 13(17):7821–7833. doi:10.1039/C0CP02869J
23. Mejía SM, Espinal JF, Mondragón F (2009) Cooperative effects on the structure and stability of $(ethanol)_3$–water, $(methanol)_3$–water heterotetramers and $(ethanol)_4$, $(methanol)_4$ tetramers. J Mol Struct THEOCHEM 901(1–3):186–193. doi:10.1016/j.theochem.2009.01.027
24. Wakisaka A, Matsuura K (2006) Microheterogeneity of ethanol–water binary mixtures observed at the cluster level. J Mol Liq 129(1–2):25–32. doi:10.1016/j.molliq.2006.08.010
25. Noskov SY, Lamoureux G, Roux B (2005) Molecular dynamics study of hydration in ethanol–water mixtures using a polarizable force field†. J Phys Chem B 109(14):6705–6713. doi:10.1021/jp045438q
26. Nishi N, Koga K, Ohshima C, Yamamoto K, Nagashima U, Nagami K (1988) Molecular association in ethanol-water mixtures studied by mass spectrometric analysis of clusters generated through adiabatic expansion of liquid jets. J Am Chem Soc 110(16):5246–5255. doi:10.1021/ja00224a002
27. Fang HL, Swofford RL (1984) Molecular conformers in gas-phase ethanol: a temperature study of vibrational overtones. Chem Phys Lett 105(1):5–11. doi:10.1016/0009-2614(84)80404-2
28. Barr-David F, Dodge BF (1959) Vapor-liquid equilibrium at high pressures. The systems ethanol-water and 2-propanol-water. J Chem Eng Data 4(2):107–121. doi:10.1021/je60002a003
29. Yang D, Wang H (2013) Effects of hydrogen bonding on the transition properties of ethanol–water clusters: a TD-DFT study. J Clust Sci 24(2):485–495. doi:10.1007/s10876-012-0514-7
30. Mejía SM, Espinal JF, Restrepo A, Mondragón F (2007) Molecular interaction of $(ethanol)_2$–water heterotrimers. J Phys Chem A 111(33):8250–8256. doi:10.1021/jp073168g
31. Lyktey MMY, DeLeon RL, Shores KS, Furlani TR, Garvey JF (2000) Migration of a proton as a function of solvation within $\{ROH\}_n\{H_2O\}H^+$ cluster ions: experiment and theory. J Phys Chem A 104(22):5197–5203. doi:10.1021/jp000872n
32. Herron WJ, Coolbaugh MT, Vaidyanathan G, Peifer WR, Garvey JF (1992) Observation of magic numbers for $(ROH)_nH_3O^+$ heteroclusters (R = CH_3, CH_3CH_2, $(CH_3)_2CH$, and $CH_3CH_2CH_2$): implications for cluster ion structure. J Am Chem Soc 114(10):3684–3689. doi:10.1021/ja00036a017
33. Pérez JF, Restrepo A (2008) ASCEC V-01: Annealing Simulado Con Energía Cuántica. Property, Development and Implementation; Grupo de Química-Física Teórica, Instituto de Química, Universidad de Antioquia, AA 1226 Medellín, Colombia
34. Schmidt MW, Baldridge KK, Boatz JA, Elbert ST, Gordon MS, Jensen JH, Koseki S, Matsunaga N, Nguyen KA, Su S, Windus TL, Dupuis M, Montgomery JA (1993) General atomic and molecular electronic structure system. J Comput Chem 14(11):1347–1363. doi:10.1002/jcc.540141112
35. Kar BP, Ramanathan N, Sundararajan K, Viswanathan KS (2012) Conformations of dimethyl carbonate and its complexes with water: a matrix isolation infrared and ab initio study. J Mol Struct 1024:84–93. doi:10.1016/j.molstruc.2012.05.007
36. Rozas I (2007) On the nature of hydrogen bonds: an overview on computational studies and a word about patterns. Phys Chem Chem Phys 9(22):2782–2790. doi:10.1039/B618225A
37. Pérez JF, Hadad CZ, Restrepo A (2008) Structural studies of the water tetramer. Int J Quantum Chem 108(10):1653–1659. doi:10.1002/qua.21615

38. Guerra D, David J, Restrepo A (2014) Hydrogen bonding in the binary water/ammonia complex. J Comput Methods Sci Eng 14(1): 93–102. doi:10.3233/JCM-140487
39. Hincapié G, Acelas N, Castaño M, David J, Restrepo A (2010) Structural studies of the water hexamer. J Phys Chem A 114(29): 7809–7814. doi:10.1021/jp103683m
40. Ibarguen C, Guerra D, Hadad CZ, Restrepo A (2014) Very weak interactions: structures, energies and bonding in the tetramers and pentamers of hydrogen sulfide. RSC Adv 4(102):58217–58225. doi:10.1039/C4RA09430A
41. Gonzalez J, Florez E, Romero J, Reyes A, Restrepo A (2013) Microsolvation of Mg^{2+}, Ca^{2+}: strong influence of formal charges in hydrogen bond networks. J Mol Model 19(4):1763–1777. doi: 10.1007/s00894-012-1716-5
42. Romero J, Reyes A, David J, Restrepo A (2011) Understanding microsolvation of Li^{+}: structural and energetical analyses. Phys Chem Chem Phys 13(33):15264–15271. doi:10.1039/C1CP20903E
43. Zapata-Escobar A, Manrique-Moreno M, Guerra D, Hadad CZ, Restrepo A (2014) A combined experimental and computational study of the molecular interactions between anionic ibuprofen and water. J Chem Phys 140(18):184312. doi:10.1063/1.4874258 (184311–184311)
44. Frisch MJ, Trucks GW, Schlegel HB, Scuseria GE, Robb MA, Cheeseman JR, Scalmani G, Barone V, Mennucci B, Petersson GA, Nakatsuji H, Caricato M, Li X, Hratchian HP, Izmaylov AF, Bloino J, Zheng G, Sonnenberg JL, Hada M, Ehara M, Toyota K, Fukuda R, Hasegawa J, Ishida M, Nakajima T, Honda Y, Kitao O, Nakai H, Vreven T, Montgomery JA Jr, Peralta JE, Ogliaro F, Bearpark M, Heyd JJ, Brothers E, Kudin KN, Staroverov VN, Kobayashi R, Normand J, Raghavachari K, Rendell A, Burant JC, Iyengar SS, Tomasi J, Cossi M, Rega N, Millam NJ, Klene M, Knox JE, Cross JB, Bakken V, Adamo C, Jaramillo J, Gomperts R, Stratmann RE, Yazyev O, Austin AJ, Cammi R, Pomelli C, Ochterski JW, Martin RL, Morokuma K, Zakrzewski VG, Voth GA, Salvador P, Dannenberg JJ, Dapprich S, Daniels AD, Farkas Ö, Foresman JB, Ortiz JV, Cioslowski J, Fox DJ (2009) Gaussian 09, Revision D.01. Gaussian, Inc, Wallingford
45. Boys SF, Bernardi F (1970) The calculation of small molecular interactions by the differences of separate total energies. Some procedures with reduced errors. Mol Phys 19(4):553–566. doi:10.1080/00268977000101561
46. Tuma C, Daniel Boese A, Handy NC (1999) Predicting the binding energies of H-bonded complexes: a comparative DFT study. Phys Chem Chem Phys 1(17):3939–3947. doi:10.1039/A904357H
47. Kitaura K, Morokuma K (1976) A new energy decomposition scheme for molecular interactions within the Hartree-Fock approximation. Int J Quantum Chem 10(2):325–340. doi:10.1002/qua.560100211
48. Su P, Li H (2009) Energy decomposition analysis of covalent bonds and intermolecular interactions. J Chem Phys 131(1):014102. doi:10.1063/1.3159673
49. Contreras-García J, Johnson ER, Keinan S, Chaudret R, Piquemal J-P, Beratan DN, Yang W (2011) NCIPLOT: a program for plotting noncovalent interaction regions. J Chem Theory Comput 7(3):625–632. doi:10.1021/ct100641a
50. Bader RFW (2002) Atoms in molecules. In: Encyclopedia of computational chemistry. Wiley, New York. doi:10.1002/0470845015.caa012
51. McQuarrie DA (2000) Statistical mechanics. University Science Books, Sausalito, CA
52. Kar BP, Ramanathan N, Sundararajan K, Viswanathan KS (2014) Matrix isolation and DFT study of the conformations of diethylcarbonate. J Mol Struct 1072:61–68. doi:10.1016/j.molstruc.2014.04.044
53. Kar T, Scheiner S (2004) Comparison of cooperativity in CH···O and OH···O hydrogen bonds. J Phys Chem A 108(42):9161–9168. doi: 10.1021/jp048546l
54. Gu Y, Kar T, Scheiner S (1999) Fundamental properties of the CH···O Interaction: is it a true hydrogen bond? J Am Chem Soc 121(40): 9411–9422. doi:10.1021/ja991795g
55. May E, Destro R, Gatti C (2001) The unexpected and large enhancement of the dipole moment in the 3,4-bis(dimethylamino)-3-cyclobutene-1,2-dione (DMACB) molecule upon crystallization: a new role of the intermolecular CH···O interactions. J Am Chem Soc 123(49):12248–12254. doi:10.1021/ja010316m
56. Kim KS, Mhin BJ, Choi US, Lee K (1992) Ab initio studies of the water dimer using large basis sets: the structure and thermodynamic energies. J Chem Phys 97(9):6649–6662. doi:10.1063/1.463669
57. Nielsen IMB, Seidl ET, Janssen CL (1999) Accurate structures and binding energies for small water clusters: the water trimer. J Chem Phys 110(19):9435–9442. doi:10.1063/1.478908
58. Xantheas SS (1994) Ab initio studies of cyclic water clusters $(H_2O)_n$, n=1–6. II. Analysis of many-body interactions. J Chem Phys 100(10):7523–7534. doi:10.1063/1.466846
59. Johnson ER, Keinan S, Mori-Sánchez P, Contreras-García J, Cohen AJ, Yang W (2010) Revealing noncovalent interactions. J Am Chem Soc 132(18):6498–6506. doi:10.1021/ja100936w
60. Thomsen DL, Axson JL, Schrøder SD, Lane JR, Vaida V, Kjaergaard HG (2013) Intramolecular interactions in 2-aminoethanol and 3-aminopropanol. J Phys Chem A 117(40):10260–10273. doi:10.1021/jp405512y